symmetry

MDPI

Article

Polyazulene-Based Materials for Heavy Metal Ion Detection. 3. (E)-5-((6-*t*-Butyl-4,8-dimethylazulen-1-yl) diazenyl)-1H-tetrazole-Based Modified Electrodes

Laura-Bianca Enache [1,2], Veronica Anăstăsoaie [1], Cecilia Lete [3], Alina Giorgiana Brotea [1], Ovidiu-Teodor Matica [1], Cristina-Andreea Amarandei [4], Jérémy Brandel [4], Eleonora-Mihaela Ungureanu [1,*] and Marius Enăchescu [2,5,6,*]

1 Department of Inorganic Chemistry, Physical Chemistry and Electrochemistry, Faculty of Applied Chemistry and Materials Science, University "Politehnica" of Bucharest, Gheorghe Polizu 1-7, Sector 1, 011061 Bucharest, Romania; laura.bianca@cssnt-upb.ro (L.-B.E.); veronica.anastasoaie@onmicrosoft.upb.ro (V.A.); alina.brotea@upb.ro (A.G.B.); ovidiu.matica@upb.ro (O.-T.M.)
2 Center for Surface Science and Nanotechnology, University "Politehnica" of Bucharest, Splaiul Independentei 313, 060042 Bucharest, Romania
3 Institute of Physical Chemistry "Ilie Murgulescu" of the Romanian Academy, 202 Splaiul Independentei, 060021 Bucharest, Romania; clete@icf.ro
4 Hubert Curien Pluridisciplinary Institute (IPHC), Université de Strasbourg/CNRS (UMR7178), 23 rue du Loess, 67087 Strasbourg, France; amarandei@unistra.fr (C.-A.A.); jbrandel@unistra.fr (J.B.)
5 S.C. NanoPRO START MC S.R.L., 041337 Bucharest, Romania
6 Academy of Romanian Scientists, 54 Spaiul Independentei, 050094 Bucharest, Romania
* Correspondence: mihaela.ungureanu@upb.ro (E.-M.U.); marius.enachescu@cssnt-upb.ro (M.E.); Tel.: +40-724-659287 (E.-M.U.)

check for updates

Citation: Enache, L.-B.; Anăstăsoaie, V.; Lete, C.; Brotea, A.G.; Matica, O.-T.; Amarandei, C.-A.; Brandel, J.; Ungureanu, E.-M.; Enăchescu, M. Polyazulene-Based Materials for Heavy Metal Ion Detection. 3. (E)-5-((6-*t*-Butyl-4,8-dimethylazulen-1-yl) diazenyl)-1H-tetrazole-Based Modified Electrodes. *Symmetry* **2021**, *13*, 1642. https://doi.org/10.3390/sym13091642

Academic Editor: Edwin Charles Constable

Received: 16 June 2021
Accepted: 2 August 2021
Published: 7 September 2021

Abstract: A recently synthesized azulene-tetrazole molecular receptor is proposed in this paper to continue the series of azulene substituted compounds that have been developed to build polyazulene-based materials for heavy metal (HM) ion detection. This study focuses on characterization of (E)-5-((6-*t*-butyl-4,8-dimethylazulen-1-yl) diazenyl)-1H-tetrazole (**L**) by electrochemical techniques in view of its use for designing electrochemical sensors for HM ion complexation. The character of redox processes was proved by cyclic, differential pulse, and rotating disk electrode voltammetry. An in-depth thermodynamic study of the complexation properties of the free ligand with Pb(II) and Cd(II) from aqueous solutions was performed, and the stoichiometry and stability constant values were determined. Chemically modified electrodes (CMEs) based on **L** (**L**-CMEs) prepared by controlled potential electrolysis (CPE) at different applied potentials and charges were characterized by cyclic voltammetry and electrochemical impedance spectroscopy (EIS). Their surface morphology was examined by scanning electron microscopy (SEM). The complexing properties of **L**-CMEs were investigated towards the detection of HM ions by anodic stripping and compared to the stability constants of the complexes in solution. Voltametric curves showed well-defined peaks for Pb (II), Cd (II), Cu (II) and Hg (II), but the responses differ from each other and vary depending on the ion concentrations in the accumulation solutions. The best results were obtained for Pb(II) and Cd(II) ions. The results obtained for Pb(II) are promising and can be used for its analysis in water solutions (detection limit of about 10^{-9} M).

Keywords: (E)-5-((6-*t*-butyl-4,8-dimethylazulen-1-yl) diazenyl)-1H-tetrazole; electrochemical techniques; modified electrodes; scanning electron microscopy; electrochemical impedance spectroscopy; heavy metal sensing; speciation; stability constants

1. Introduction

For human safety, it is extremely important to monitor the HM ions that are present in water and food [1–4]. Numerous health problems have been reported associated with prolonged exposure to metal ions such as Pb (II), Cd (II) and Hg (II) due to their tendency to

accumulate. Such HMs accumulate continuously in ecosystems due to industrial processes such as combustion. It is very important to develop new techniques for the detection of low levels of HM ions, especially on-site.

On-site analysis of HM ions present in water or food requires methods with high sensitivity and accuracy. A modern alternative to these methods can be based on electrochemical sensors [5], which can be portable and could have rapid response and high sensitivity [6,7]. Electrochemical sensors based on CMEs [8] could bring more sensitivity and selectivity in comparison to other spectroscopic or optical techniques [9]. They can be included in portable devices allowing on-site monitoring of HMs. The combination of modern electrochemical techniques with developments in the field of microelectronics and miniaturization allows the introduction of high-performance and reliable electrical devices for efficient control of processes or pollution. This makes electrochemical measurements possible on the spot and in real time [10].

Considering the advantages of CMEs and our goal of detecting HMs, it is important to search for new molecules that lead to the obtention of new types of sensors. To make this possible, they must contain a metal ion complexing unit and a moiety that is capable of electropolymerization [11,12].

Previous studies performed in our team have highlighted the possibility of using azulene derivatives to obtain modified electrodes for HM dosing [13]. The complexing units were based on pyridine [14], tetrazoles [13,15], thiadiazoles [16], etc. Among the most recent results [13], there are tetrazoles that have quite low detection limits (less than 5×10^{-8} mM).

The affinity of a ligand for a given metal is dependent on the ligand (type of coordinating groups, denticity, geometry, flexibility, steric hindrance, etc.) and on the metal (coordination number, coordination sphere). For example, the d^{10} Cd (II) ion in group 12 is of particular interest due to its large radius and strong interaction with different simultaneous donors, as well as multiple ways of coordination and luminescence properties. The Cd(II)-tetrazole clusters that have been mentioned in reports so far have been harvested with tetrazole derivatives substituted by hydroxy, amino, methyl or carboxyl groups [17–19]. In most cases, cadmium centres have six-coordinated octahedral geometries, and the pyramidal/trigonal square bipyramid has five coordinates. However, a bipyramidal pentagonal stereochemistry with seven coordinates is also observed. To the best of our knowledge, only one example of a Pb-cluster with tetrazole derivative has been prepared and characterized for its chemical structure and properties [20]. After the accidental discovery of the first tetrazole complex, tetrazole derivatives with four nitrogen-electron-donating atoms as ligands have attracted more and more attention. Pb(II) presents a large radius, flexible coordination mode and variable stereochemical activity, which are ascribed to its lone electron pair ($6s^2$). Based on the disposition of ligands around the metal ion, the terminology assigned was described as holo-directed (the bonds with the ligand atoms are directed over the entire surface of a globe) and hemi-directed (the bonds with the ligand atoms are directed over a certain part of the globe surface). Consequently, there is an identifiable void (or gap) in the distribution of bonds to the ligands [21]. The geometry seems to strongly depend on the coordination number (CN) of Pb(II) and on the steric repulsion of the ligands. Consequently, according to [21], the geometry of the Pb atom in Pb (II) complexes is either hemi-directed (for CNs between 2 and 5) or halo-directed (for high CNs of 9–10). For intermediate CNs (from 6–8), both types of coordination were detected. As these metals can accept several CNs, it is important to study the coordination properties of new ligands to understand the coordination mechanism.

In the present paper are given the results obtained when testing HMs' detection using CMEs based on (E)-5-((6-*t*-butyl-4,8-dimethylazulen-1-yl) diazenyl)-1H-tetrazole (**L**). The presence of extra methyl and *t*-butyl groups grafted on the azulene ring at positions 4,8 and 6, respectively (Figure 1) increases the electron density on the azulene nucleus, which is a favourable premise for the better complexation of metal ions, which our research group is pursuing in our experiments. To evaluate the effect of the ligand **L** immobilization on the

electrode surface upon its ability to complex HMs, complexation studies of the free ligand in solution were carried out.

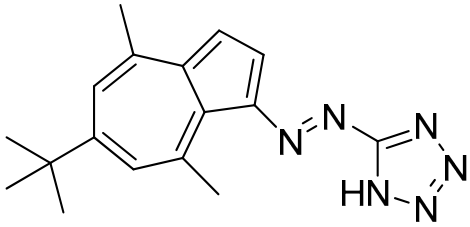

Figure 1. Structure of **L**.

2. Materials and Methods

The compound **L** was synthesized according to previously described methods [22]. Acetonitrile (CH_3CN, Sigma Aldrich, electronic grade 99.999% trace metals) and tetrabutylammonium perchlorate (TBAP, Fluka, Munich, Germany, analytical purity ≥99.0%) were used as received.

The salts containing metal cations were mercury (II) acetate (Fluka, Munich, Germany, ≥98%), cadmium nitrate tetrahydrate (Fluka, Munich, Germany, ≥98%), copper (II) acetate monohydrate (Fluka, Munich, Germany, ≥98%) and lead (II) nitrate (Fluka, Munich, Germany, ≥99.5%). HM solutions with different concentrations were prepared by successive dilution from 10^{-3} M stock solutions.

All electrochemical measurements were performed using a potentiostat Autolab 302N connected to cells with three electrodes. For electrochemical characterization and CME preparation, the working electrode was a glassy carbon (GC) disk of 3 mm diameter (Metrohm, Herisau, Switzerland), a platinum wire was the counter electrode and Ag/10 mM $AgNO_3$, 0.1M TBAP/CH_3CN was the reference electrode. All potentials were referred to the potential of the ferrocene/ferrocenium redox couple (Fc/Fc^+) in 0.1 M TBAP/CH_3CN. The electrochemical detection of HM ions from aqueous solutions was carried out using another three-electrode cell (transfer cell) in 0.1 M buffer acetate (pH = 4.5) as a supporting electrolyte according to the procedure already described [13,15]. In this cell, the working electrodes were the GC disks modified with **L** films, the reference electrode was Ag/AgCl, 3 M KCl and the auxiliary electrode was a platinum wire.

EIS experiments were performed by means of an Autolab potentiostat/galvanostat 302N (Ecochemie, The Netherlands) that included the FRA2 impedance module. EIS measurements were accomplished on the frequency range between 100 kHz and 50 MHz by applying a potential with the amplitude of 10 mV over the dc potential of 0.19 V (OCP) in 0.1 M TBAP/CH_3CN solution containing 5 mM ferrocene redox couple. The impedance data are presented in the form of Nyquist plots. EIS spectra were processed using Z View 2.4 software from Scribner Association Inc., Derek Johnson.

The electrochemical characterization of **L** and its corresponding polymer was performed by cyclic voltammetry (CV) to establish the processes nature, differential pulse voltammetry (DPV) to find the right values of peak potentials and rotating disk electrode voltammetry (RDE) to estimate the number of electrons involved in the processes [13,23,24]. The surface of the GC working electrode was polished before each determination with diamond paste and cleaned with acetonitrile. The electrochemical characterization of **L** was performed at 25 °C under argon atmosphere.

CMEs were prepared from millimolar solutions of **L** in 0.1 M TBAP/CH_3CN by CPE. Then each **L**-CME was washed with acetonitrile and introduced in 0.1 M acetate buffer solution (pH = 4.5) where it was equilibrated and overoxidized as previously described [13,15]. The resultant electrode, named further "**L**-CME" was immersed for 15 min under stirring in a synthetic test solution of HM ions. After this procedure, the modified electrode with accumulated HM ions was taken out and cleaned with deionized water. The last electrode was immersed in a cell containing 0.1 M acetate buffer solution

(pH = 4.5). Here, it was polarized for 3 min at −1.2 V, and then the DPV curves were recorded between −1.2 and +0.8 V.

A Hitachi SU 8230 (Tokyo, Japan) was used for SEM measurements. CME preparation for SEM was done on working GC disk electrodes (Metrohm, Herisau, Switzerland) with 6 mm diameter.

The complexation properties were studied by UV–visible spectrophotometry (JASCO V-670) in 1 cm path length quartz cuvettes in freshly dried acetonitrile at a constant ionic strength of 0.1 M TBAP. Aliquots of a metal solution were added to an **L** solution (4 < [L] < 15 μM) and a UV–visible spectrum (200–700 nm) was recorded after each addition. A calibration curve was used for each set of data to precisely determine the **L** concentration. The stoichiometry of the metallic complexes and the equilibrium constants were determined by fitting the spectrophotometric data with HypSpec 2008 software [25]. The computer program Hyperquad Simulation and Speciation (HySS 2009) was used to obtain the species distribution curves [25,26].

3. Results

3.1. Electrochemical Characterization of **L**

The electrochemical characterization of **L** was performed for different millimolar concentrations of **L** by CV, DPV and RDE. The oxidation and reduction curves were obtained in solutions containing TBAP in CH_3CN. The curves were recorded starting from the equilibrium potential as shown in Figures 2–5 (the arrows mark the direction in which the potential was swept away). The curves for the supporting electrolyte are drawn with dotted lines.

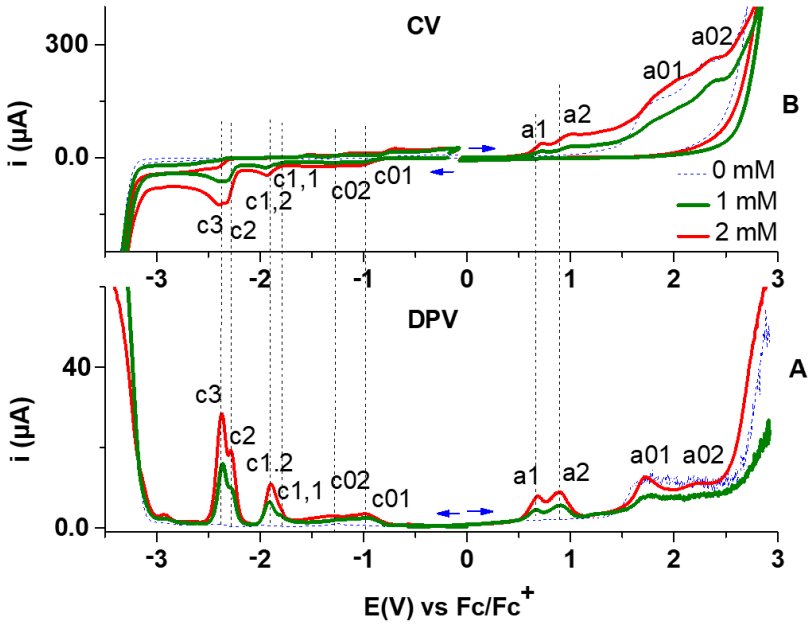

Figure 2. DPV (**A**) and CV (**B**) curves on GC for **L** in 0.1 M TBAP/CH_3CN at different concentrations (mM): 0 (dotted blue line), 1 (green line), 2 (red line); DPV currents are in absolute values.

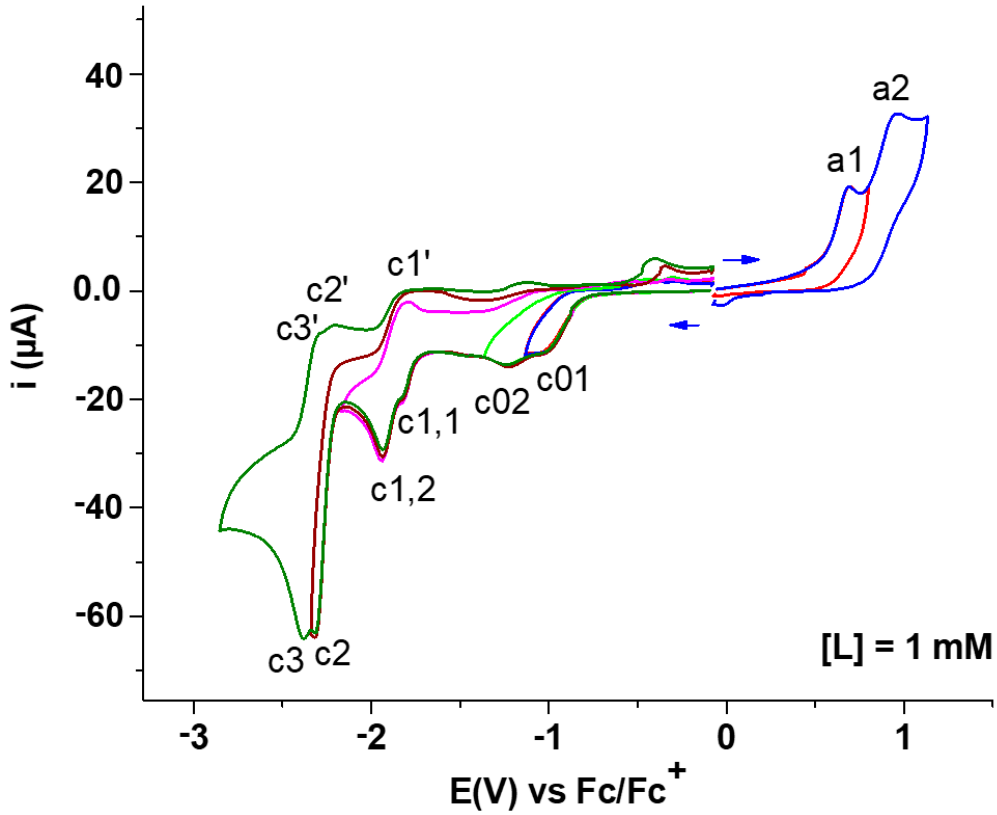

Figure 3. CV curves (0.1 V s^{-1}) on GC electrode on different potential domains for **L** (1 mM) in 0.1 M TBAP/CH_3CN.

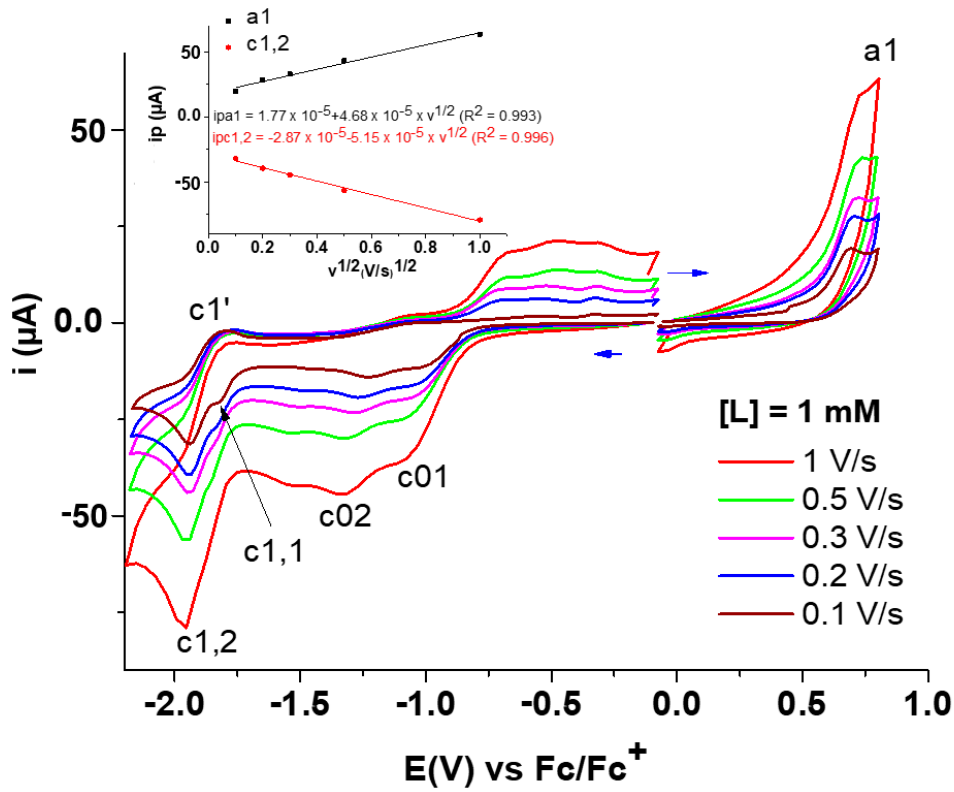

Figure 4. CV curves on GC electrode in **L** solution (1 mM) in 0.1M TBAP/CH_3CN at different scan rates; Inset: Linear dependence of current peaks vs. the square root of the scan rate for the processes corresponding to a1 and c1,2.

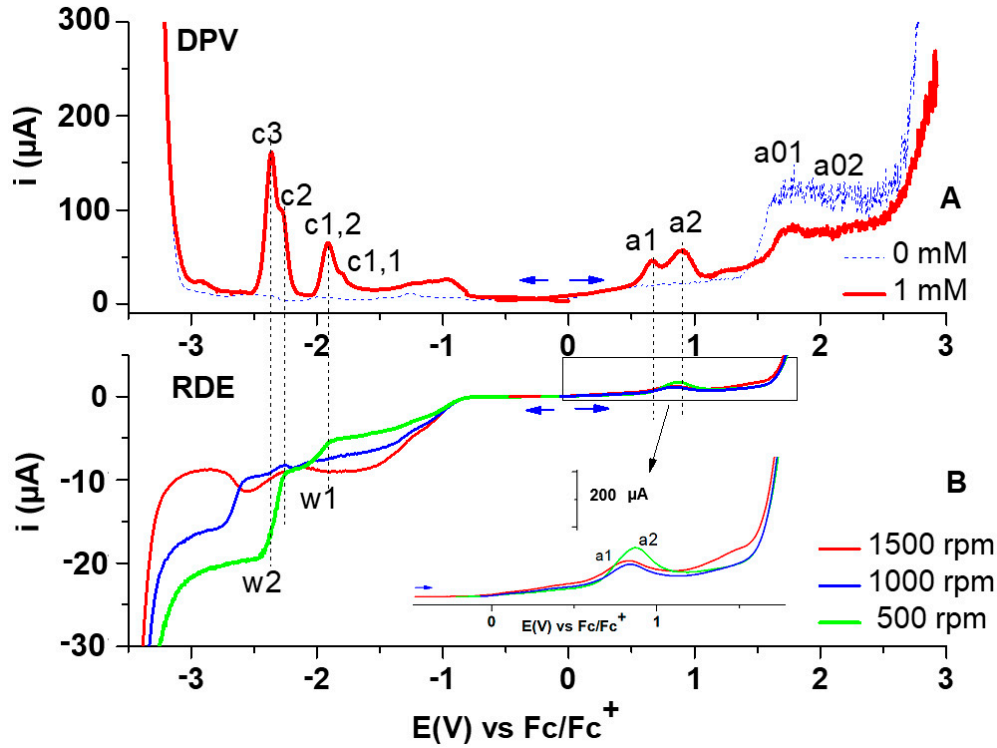

Figure 5. DPV (**A**) and RDE (**B**) curves at different rotation rates (rpm) for **L** (1 mM) on GC in 0.1 M TBAP/CH_3CN.

The oxidation and reduction DPV curves (Figure 2A) show two anodic peaks (denoted a1 and a2) attributed to **L** oxidation, and two secondary peaks (a01, a02) in the oxidation domain of the supporting electrolyte. In the cathodic domain, four peaks (denoted c1,1, c1,2, c2 and c3) are noticed for **L** reduction. The names given for the processes highlighted by DPV have been retained in CV and RDE.

The CV oxidation and reduction curves given in Figure 2B show in the anodic scans two main processes corresponding to a1 and a2 peaks from DPV and two secondary peaks (a01, a02) in the oxidation domain of the solvent. In the cathodic scans, four peaks are seen for **L** reduction corresponding to c1,1, c1,2, c2 and c3 from DPV.

The anodic and cathodic DPV and CV currents increase with the concentration of **L**.

The CV curves on different potential ranges are plotted in Figure 3, and the CV curves on the potential ranges of the first anodic (a1) and cathodic (c1,1 and c1,2) peaks at different scan rates are plotted in Figure 4.

The electrochemical processes highlighted by CV and DPV oxidation and reduction curves have the characteristics given in Table 1. Based on the shape of CV peaks from Figures 3 and 4 recorded on different potential ranges and at different scan rates, it can be appreciated that peaks a1 and a2 correspond to irreversible processes, while c1,1, c1,2, c2 and c3 correspond to reversible processes. Anodic and cathodic CV and DPV peak currents increase with the concentration of **L**. Based on these variations, the calibration curves can be obtained.

The values of the peak potentials from the CV and DPV curves from Table 1 agree with the values previously found for the unsubstituted ligand [13]. The potential of the first oxidation peak (a1) for **L** is +0.72 V. This value is 0.19 V lower than that reported for the unsubstituted compound [13] for which the potential of the first oxidation peak is +0.91 V. It means that **L** is oxidized more easily than the unsubstituted azulene derivative. These values are consistent with the electron repelling inductive effects of alkyl groups grafted on the azulene moiety of **L**. Considering the **L** structure (that has a polarized azulene moiety), the first oxidation peak corresponds to the process of a radical cation formation, which is

followed by polymerization reactions leading to a polymeric film, as has been seen also in case of other azulene compounds [13,15].

Table 1. Potential (in V) of anodic (a) and cathodic (c) peaks from CV and DPV curves recorded in 1 mM solution of **L** in 0.1M TBAP/CH_3CN and the features of associated processes resulting from the CV curves obtained on different potential domains and at different scan rates.

Peak	Method		Process Reversibility
	CV	DPV	
a1	0.72	0.66	Irreversible
a2	1.00	0.90	Irreversible
c1,1	−1.77	−1.80	Reversible
c1,2	−1.95	−1.92	Reversible
c2	−2.314	−2.27	Reversible
c3	−2.383	−2.35	Reversible

The signals c01 and c02 obtained when scanning to small negative potentials (−1.2–−1.4 V) are due to the reduction of oxygen traces (secondary process) from residual water. The two peaks (c1,1 and c1,2) that occur during the cathodic scans can be attributed to the ligand because they increase as the ligand concentration increases. They are due to the reduction of the azo double bond that connects the azulene and tetrazole moieties. This reduction process has an ECE mechanism and occurs with two electrons and two protons, with the electron transfers taking place at very close potentials as in the case of other azo azulenes [13]. The electrochemical steps of the mechanism (two peaks) can be distinguished only at lower (than 0.1 V/s) scan rates. The azo bond reduction is the most probable reaction for a ligand with this structure, and it occurs at the potential of −1.95 V. In case of the unsubstituted derivative, this reduction occurs at −1.8 V [13]. The peaks' potential values obtained for **L** in comparison with those for the unsubstituted derivative are explained by the effects of extra alkyl groups that increase the electron density on the azulene nucleus, pushing the oxidation/reduction potential of the **L** azulene moiety to lower/higher potentials (oxidation occurs easily and reduction is harder).

The RDE curves recorded at different rotation rates on the GC electrode are plotted in Figure 5 in parallel with DPV curves for **L** in the supporting electrolyte. The correspondence between the processes put in evidence by these two methods has been shown by vertical dotted lines. Very small values of RDE currents on all anodic ranges can be noticed (the current drops to the baseline at potentials higher than that for the a1 peak).

The electrochemical processes put in evidence by RDE (Figure 5) agree with the processes evidenced by CV and DPV. In the cathodic RDE scans at 500 rpm (green curve), two main waves are seen: w1, which corresponds to the two DPV closely spaced processes involved in azo group reduction (c1,1 and c1,2); and w2, which corresponds to the DPV processes c2 and c3 evidenced in the curves for **L** reduction (cathodic scans). The RDE curves for different rotation rates (500–1500 rpm) were compared in Figure 5. A different influence of the rotation rate on the limiting currents of the cathodic waves, w1 and w2, was noticed. The w1 reduction wave limiting current increases (regular dependence) with the rotation rate, while w2 decreases when the rotation rate increases. To rationalize this behaviour, a comparison with DPV curves (presented at the top of Figure 5) was done. The waves w1 and w2 are distinct at 500 rpm, and they involve a number of electrons in the ratio of 1:3 (measured on the green curve). This ratio is in agreement with the proposed mechanism for the reduction processes of the unsubstituted azulene derivative [13]. At 1000 rpm, this ratio is quite the same, but the limiting currents for w1 and w2 are lower. At a rotation rate of 1500 rpm, they are even lower. This unusual variation of the w2 wave with the electrode rotation rate increase can be attributed to the parallel formation of an insulating polymer film, a process that occurs in this range of potential. The film formation leads to electrode coverage and explains the drop of the current. This cathodic polymerization process is known for azulene derivatives [24].

The noticed drop of the current with the increase of the electrode rotation rates can be rationalized by **L** polymerization by electroreduction, as in the case of the corresponding unsubstituted azulene [13]. If the rotation rate is increased from 500 rpm to higher rates of 1000 and 1500 rpm, the film deposition is not favoured, and the current drops in comparison with the current at 500 rpm, in agreement with the obtained cathodic curves in Figure 5.

In the anodic scans, very small variations of the RDE currents with the rotation rate of the electrode can be noticed in the anodic range corresponding to the DPV peaks a1 and a2 (see the insertion in the RDE curves in Figure 5). From this inset, it can be seen that, after the a2 peak, the RDE current decreases and reaches the background value at the potential of +1.3 V. This shape of the RDE anodic curves with very low values of RDE currents at all electrode rotation rates can be attributed to the formation of insulating polymer films (which lower the current to the baseline). These films are formed by anodic electropolymerization, as will be proven below. If the electrode rotation rate is higher, film deposition on the electrode is not favoured. Consequently, the oxidation processes of the supporting electrolyte appear more intense (for instance, at 1.5 V $i_{RDE,\ 1500\ rpm} > i_{RDE,\ 500\ rpm}$). Such behaviour indicates the formation of insulating films, as in the case of unsubstituted azulene, which has similar behaviour [13]. The potential value of +1.3 V, which is an electrochemical isosbestic point (at which the limiting currents are equal for 500, 1000 and 1500 rpm), was chosen for the preparation of modified electrodes for HM ions recognition experiments.

3.2. Preparation of Modified Electrodes and Their Electrochemical Characterization

The CMEs were obtained by CPE in millimolar solutions of **L** in 0.1 M TBAP/CH_3CN according to previously published procedure [13,15] at different oxidation potentials established by CV measurements. These potentials were located before the processes a1 (+0.5 V) and ata2 peak (+0.8 V) and after the process a2 (+1.3 V). The modified electrodes were characterized in supporting electrolyte solution having as redox probe 5 mM ferrocene using CV (Figure 6A and Figure S1, Table S1) and EIS (Figure 6B). The cyclic voltammograms recorded for unmodified and modified GC electrodes are shown in Figure 6A, and their EIS curves are compared in Figure 6B for CMEs obtained at +1.3 V.

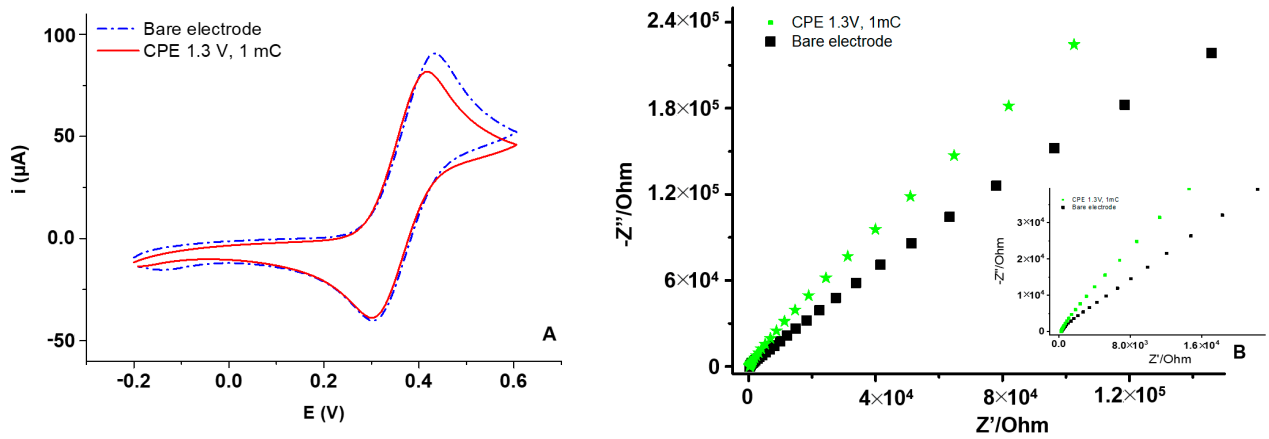

Figure 6. (**A**) CV curves recorded at 0.1 V/s for modified (continuous line) and unmodified (dashed line) GC electrode in 5 mM ferrocene in 0.1 M TBAP/CH_3CN at. (**B**) EIS curves recorded for modified (green) and unmodified (black) GC electrode in 0.1 M TBAP/CH_3CN; (**B**, inset) detail for the field with low impedances.

When testing the obtained CMEs by ferrocene redox probe, the modified electrode was transferred into a millimolar ferrocene solution in the supporting electrolyte (0.1 M TBAP/CH_3CN). The obtained CV curve (shown in Figure 6A) had small changes in comparison with that recorded for the bare electrode (dashed line). Very small changes of the CV curves were also found for the modified electrode prepared by CPE at other

potentials (+0.8 and +1.08 V) as seen in Figure S1 and Table S1, even if visual examination of the electrodes indicated the films' formation, which was confirmed by SEM.

The EIS curves for CMEs shown in Figure 6B support the presence of polymeric films deposited on the electrode surface at +1.3 V. A similar behaviour was noticed for the films prepared at +0.5 and +0.8 V. Each Nyquist plot supposes semicircular and linear regions. The semicircular region recorded at higher frequencies corresponds to a limiting electron transfer process, and its diameter to the electron-transfer resistance (R_{ct}), which controls the electron transfer kinetics at the electrode interface. The Nyquist plots for electrodes unmodified by the polymeric film and for modified GC electrodes obtained at +1.3 V were recorded at +0.3 V and are exhibited in Figure 6B. As can be seen, the imaginary part of the impedance (−Z″) is higher for the spectrum of the modified GC electrode than that of the unmodified GC electrode, confirming the covering of the electrode after electropolymerization. This result agrees with the results obtained by CV (Figure 6A).

For the films prepared at +0.8 and +1.3 V, the following electrochemical parameters were calculated (Table 2): number of electrons, n, involved in the oxidation of a monomer unit (Equation (1)); thickness of the polymeric film, g (Equation (2)); surface coverage by the film, Γ (Equation (3)) and charge transfer conductivity, D (Equation (4)). In Equation (1), $\Delta E_{p1/2}$ were calculated from the DPV curves (Figure S2) of the films transferred in the supporting electrolyte (0.1 M TBAP/CH_3CN), R = 8.314 J/mol K, T = 298 K, F = 96,500 C/mol. In Equation (2), q_{pol} is the charge used in CPE, $M_{monomer}$ is the monomer molar mass, ρ is the density of the polymer films (which have been approximated to 1 g/cm^3) and A is the electrode area (cm^2). The GC electrodes used for CPE have a diameter of 3 mm and a surface area of 0.071 cm^2. In Equation (3), Q is the anodic charge consumed in the p-type doping process (equal to the area of the CV oxidation peak in Figure S3), and the other quantities have the meanings given previously. In Equation (4), R_{ct} is the charge transfer resistance through the film, calculated from the impedance measurements of the film in the supporting electrolyte at equilibrium potential.

$$\Delta E_{p1/2} = \frac{3.53 \cdot R \cdot T}{n \cdot F} \tag{1}$$

$$g = \frac{q_{pol} \cdot M_{monomer}}{n \cdot F \cdot A \cdot \rho} \tag{2}$$

$$\Gamma = \frac{Q}{n \cdot F \cdot A} \tag{3}$$

$$D = \frac{g}{R_{ct} \cdot A} \tag{4}$$

Table 2. Characteristics obtained from DPV and EIS for the films (F1 and F2) prepared at different potentials by CPE.

Crt. Nr.	Potential for L-CME Preparation by CPE	q_{pol} (mC)	$\Delta E_{p1/2}$ (mV)	R_{ct}	n	g (µm)	$\Gamma \times 10^7$ (mol/cm^2)	$D \times 10^7$ (Ω/cm)
F1	0.8 V	0.725	180	4340	0.5	0.65	2.12	2.11
F2	1.3 V	1	94	4467	1	0.45	1.46	1.42

Table 2 gives the main parameters for the films prepared at +0.8 and +1.3 V. At +0.5 V, the film is formed with difficulty by CPE. The deposition time was much longer (several hours) for the same polymerization charge (1 mC, corresponding to 14 mC/cm^2) than at higher potentials (about 30 min for +0.8 V, and 8 min for +1.3 V). That is why the films prepared at +0.8 and +1.3 V were analysed for practical reasons, and their parameters were calculated from DPV (Figure S2), CV (Figures S3 and S4 that confirm the linear dependence of peak currents on the scan rate for the films) and EIS curves. From Table 2, it is observed that the number of electrons, n, involved in the oxidation of a monomeric unit is 0.5 for the film prepared at +0.8 V (F1) compared to 1 for the one prepared at +1.3 V (F2). This

indicates two different structures of the formed films. The F1 film is thicker (g F1 = 0.65 μm > g F2 = 0.45 μm) and has a higher surface coverage: Γ (F1) = 2.12 × 10^{-7} mol/cm^2 > Γ (F2) = 1.46 × 10^{-7} mol/cm^2. This film is also more conductive than the film prepared at +1.3 V: D (F1) > D (F2).

3.3. Modified Electrodes' Surface Characterization by SEM

SEM measurements were performed at different magnifications on **L**-CMEs prepared at different potentials and at the same polymerization charge [13,16]. The influence of the potential on the morphology of the films prepared at three significant potentials (+0.5, +0.8 and +1.3 V) is presented in Figure 7.

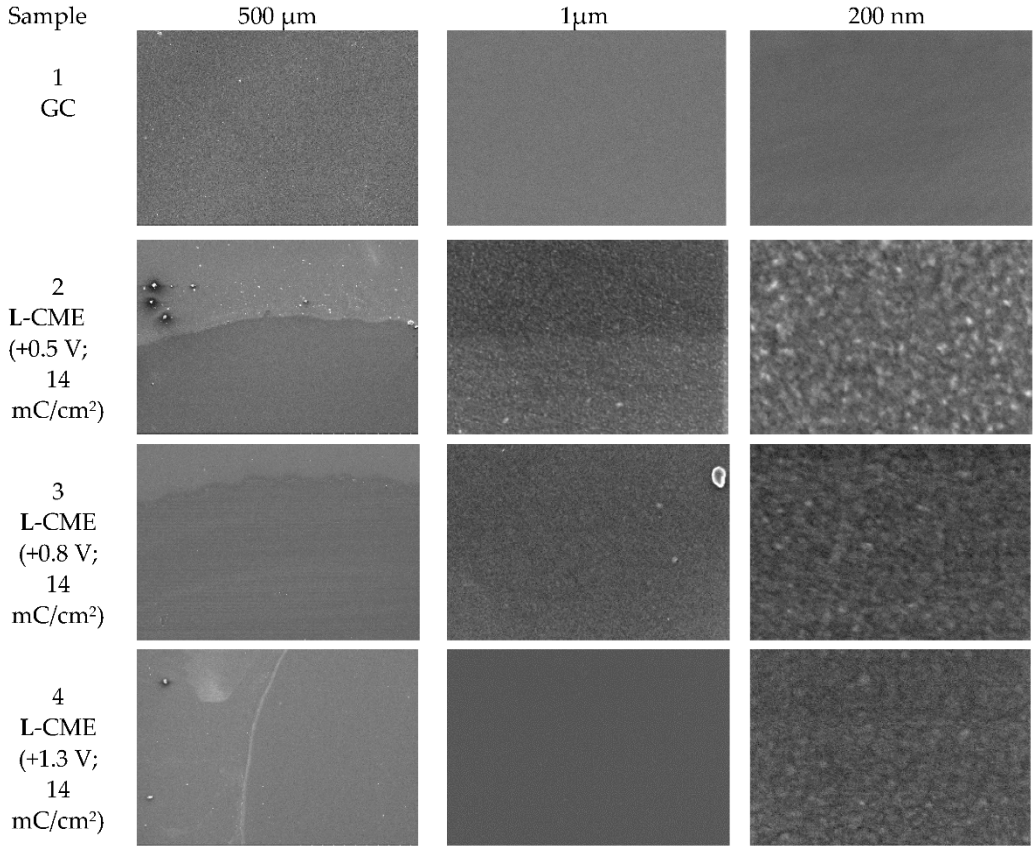

Figure 7. SEM micrographs at different magnifications for films obtained by CPE at different potentials (0, +0.5, +0.8 and +1.3 V) and using the same polymerization charge (14 mC/cm^2).

SEM measurements at various magnifications confirmed the formation of films in case of **L**-CMEs preparation by electropolymerization (Figure 7). From the magnification at 200 nm, the films are uniformly deposited on the surfaces. SEM images are different for the films prepared by CPE at various potentials. For the film prepared at +0.5 V (line 2), there are areas (in white) with more prominent columnar formations, which indicate the presence of a thicker film than those obtained at +0.8 V (line 3) and +1.3 V (line 4). These features were also confirmed by the visual images of the electrodes' coatings, which showed a green film at +0.5 V, having other appearance and colour than those obtained at +0.8 and +1.3 V. The different morphology of the films prepared at +0.5, +0.8 and +1.3 V noticed by SEM confirmed the results obtained by CV, DPV, RDE and EIS concerning the influence of the preparation potential on the films' properties.

3.4. Recognition of Heavy Metal Ions Using **L**-*CMEs*

For HM ion recognition, **L**-CMEs were obtained by CPE at +1.3 V in 1 mM solution of **L** in 0.1 M TBAP/CH_3CN using a charge of 14 mC/cm^2. They were tested by the procedure

already described [13,15]. After preparation and cleaning with acetonitrile, the modified electrodes were immersed in acetate buffer (0.1 M) at pH 4.5 and cycled for equilibration and overoxidation. The obtained electrodes (denoted **L**-CMEs) were immersed in synthetic solutions in water containing a mixture of HM ions under magnetic stirring for 10 min, then they were polarized at −1.2 V (3 min) in acetate buffer (pH 4.5) to reduce the accumulated cations, and finally linearly swept in anodic scans using DPV (Figure 8A).

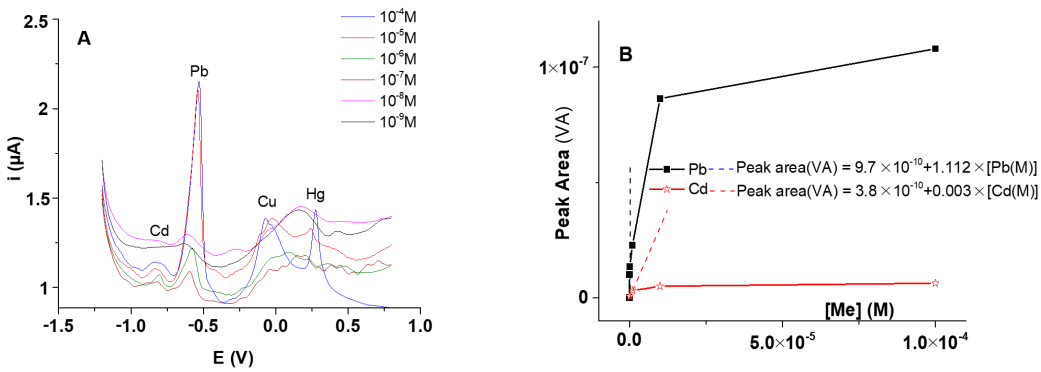

Figure 8. (**A**) DPV stripping curves in acetate buffer at pH 4.5, measured in mixtures of equal concentrations of HMs; (**B**) dependence of DPV peak current areas for each metal (Me) on metal ion concentration [Me] in tested water solutions; equations of the linear domains are given for Pb and Cd; **L**-CME were obtained by CPE (+1.3 V, 14 mC/cm^2) in 1 mM solution of **L** in 0.1 M TBAP/CH_3CN.

Peaks for Cd, Pb, Cu and Hg dissolution were noticed successively at the potentials of −0.818, −0.528, −0.075 and +0.276 V, respectively. The DPV stripping peak currents were recorded and examined for each ion vs. HM ion concentration [Me] in accumulation solutions. The peak areas for Pb and Cd ions that shown the highest signals have been plotted vs. metal ion [Me] concentration (Figure 8B). The linear parts of these calibration curves are shown with dashed lines, and their equations are given in Figure 8B.

The DPV curves show striping peaks for all investigated ions (Table 3), indicating that these ions have been retained by complexation in the polymeric films. Their heights are very different, showing a selective complexation for certain ions, such as Pb and Cd. Their plots show linear parts (dashed lines) at low concentrations. The stripping currents for Pb are by far the highest among the other peaks. The slope of 1.112 VA/M indicates a greater sensitivity for this HM ion. This estimated detection limit for Pb is 50 times lower than that obtained using the corresponding unsubstituted azulene ligand for the CMEs' preparation [13]. It is also about 10 times lower than that obtained when using a similar ligand but differently substituted with alkyl groups [15]. These variations in Pb sensitivity obtained by CMEs prepared with differently substituted ligand structures show that the structure of the ligand is an essential factor in obtaining superior recognition parameters.

Table 3. Experimental **L**-CMEs parameters estimated from Figure 8.

Target	Estimated LOD (M)	Linear Detection Range (M)	Sensitivity (VA/M)
Cd(II)	10^{-7}	10^{-7}–10^{-6}	0.003
Pb(II)	10^{-9}	10^{-9}–10^{-8}	1.112
Cu(II)	10^{-5}	-	-
Hg(II)	10^{-4}	-	-

The dependence of Pb DPV peak currents is linear for concentrations of Pb(II) between 10^{-9} and 10^{-8} M. The signal for Pb(II) for **L**-CMEs is visible at 10^{-9} M, but the detection limit could be optimized especially by variation of the **L**-CMEs' preparation potential. The slope of Cd DPV peak current vs. Cd(II) concentration in accumulation solution is much lower than that for Pb (Table 3). The signals for Cu and Hg appear only when their

concentrations in accumulation solutions overcome 10^{-5} and 10^{-4} M, respectively. These values indicate a high selectivity of **L**-CMEs with respect to Pb ions vs. Cd, Cu and Hg ions. The investigation is in progress.

3.5. Complex Formation and Species Distribution in Solution

In order to evaluate the effect of immobilizing ligand **L** on the electrode on its HM complexing ability, complexation studies of Pb and Cd by the free azulene azo-tetrazole derivative **L** were carried out in solution by means of UV–vis spectrophotometric techniques. In these conditions, no precipitation was observed. These studies allowed the determination of $M_pL_q^{(2p-q)}$ (M = Cd(II) or Pb(II)) species with different stoichiometry, depending on the behaviour of the metal under study [20,21]. The models were chosen so as to be as simple and probable as possible taking into account the percentages of complex formation and statistical parameters (standard deviation on equilibrium constants and on the fitting values of the systems).

The UV–visible spectrum of ligand **L** showed three main absorption bands at 235, 317 and 445 nm (Figure 9). Upon addition of Cd(II), all three bands underwent a hypochromic shift and the band at 445 nm also shifted hypsochromically to 425 nm.

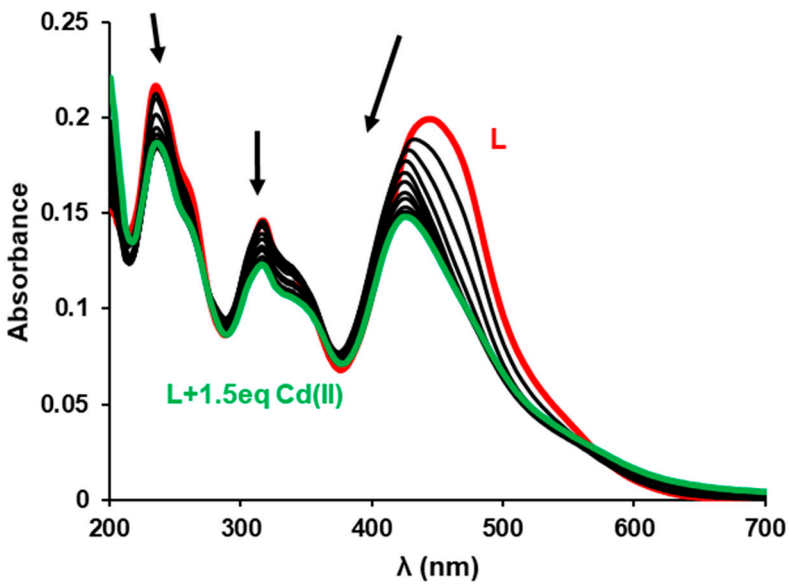

Figure 9. UV–visible batch titration of **L** ligand by Cd(II). Solvent: CH_3CN (0.1 M TBAP), T = 25 °C, [L] = 5.35 μM and 0 < [Cd]/[L] < 1.5.

Analysis of the spectral variations suggested the formation of two species and the best model was obtained for the formation of CdL_2 and CdL_3 species. The overall stability constants (logβ) for CdL_2 and CdL_3 were respectively calculated to be 12.87(3) and 18.43(6) (Table 4). The stability constants of the species allowed the calculation of the electronic spectra (Figure 10A) and the distribution curves of the species (Figure 10B).

Table 4. Experimental overall/stepwise stability constants of M^{2+}/L systems, determined in CH_3CN, 0.1 M TBAP at 25 °C.

M	logβ_{11}	logβ_{12}	logβ_{13}
Cd(II)		12.87(3)	18.43(6)
Pb(II)	6.55(1)	12.36(7)	17.86(8)

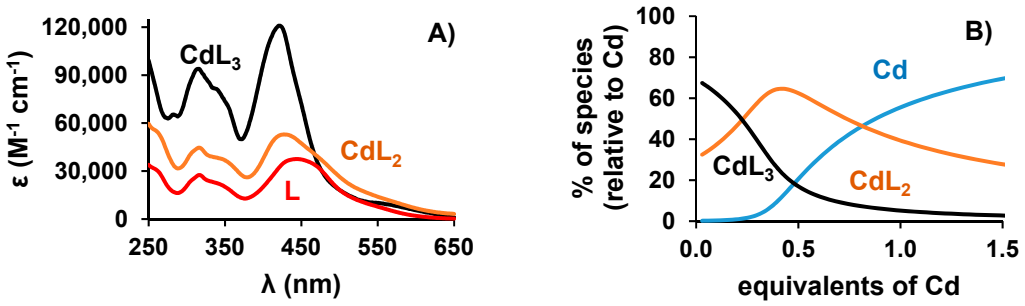

Figure 10. (**A**) Electronic spectra and (**B**) distribution curves of the Cd(II)/L complexes. Solvent: CH_3CN (0.1 M TBAP), T = 25 °C, [L] = 5.134 μM and 0 < [Cd]/[L] < 1.5.

Upon addition of Pb(II), as for Cd(II), all three absorption bands of the **L** ligand underwent a hypochromic shift, and the band at 445 nm also shifted hypsochromically to 425 nm (Figure 11). Two isosbestic points appeared, which suggested the formation of several species.

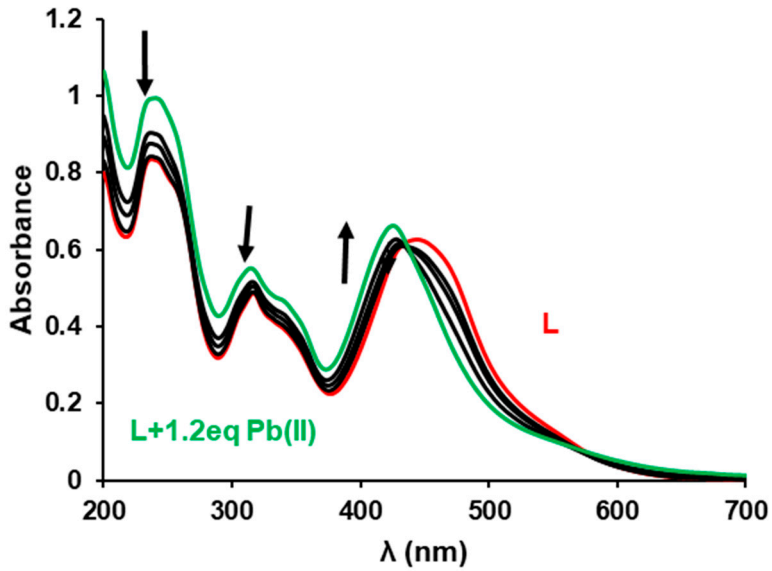

Figure 11. UV–visible batch titration of **L** ligand by Pb(II). Solvent: CH_3CN (0.1 M TBAP), T = 25 °C, [L] = 15.32 μM and 0 < [Pb]/[L] < 1.2.

Analysis of the spectral variations suggested the formation of three species, and the best model was obtained for the formation of PbL, PbL_2 and PbL_3 species. The average overall stability constants (logβ) are given in Table 4. The stability constants of the species allowed the calculation of the electronic spectra (Figure 12A) and the distribution curves of the species (Figure 12B).

The complexation studies in solution showed the formation of M**L** and M$\mathbf{L}_2$ species for Cd(II) and M**L**, M$\mathbf{L}_2$ and M$\mathbf{L}_3$ species for Pb(II). The fitting of the data did not suggest the formation of higher coordinated species as often observed for these metals, probably due to steric hindrance of the azulene moiety.

The low metal concentrations used in the **L**-CME experiments would correspond to a high ligand to metal ratio where, according to the species distribution curves in solution (Figures 10B and 12B), the M$\mathbf{L}_2$ and M$\mathbf{L}_3$ species would be dominant. The stability constants of these species (Table 4) showed that, in solution, ligand **L** has a slightly higher affinity for Cd(II) than for Pb(II). The experiments on the **L**-CME highlighted, on the contrary, a high selectivity for Pb(II) vs. Cd(II). This very different behaviour results from the immobilization of the ligand on the electrode by electropolymerization. This immobilization no longer

allows the ligands to arrange freely around the metal as in solution, resulting in strong differences in the coordination properties such as the appearance of selectivity, in that case.

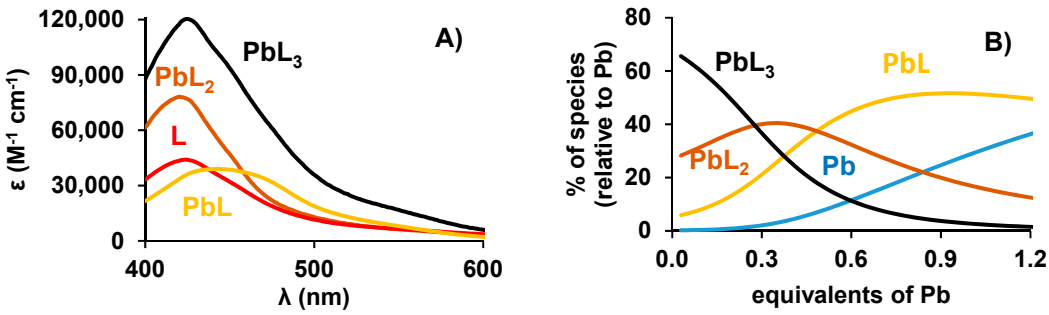

Figure 12. (**A**) Electronic spectra and (**B**) distribution curves of the Pb(II)/L complexes. Solvent: CH_3CN (0.1 M TBAP), T = 25 °C, [L] = 7.91 μM and 0 < [Pb]/[L] < 1.2.

4. Conclusions

We successfully prepared **L**-CMEs based on (E)-5-((6-*t*-butyl-4,8-dimethylazulen-1-yl) diazenyl)-1H-tetrazole (**L**). Their characterization by electrochemical techniques revealed the covering of the modified electrodes with polymeric films with different conductivity and concentrations of complexing centres on the electrode surface. CV, DPV, RDE, EIS and SEM methods confirmed the variation of the morphological properties of the films prepared at different potentials.

The ability of **L**-CMEs to complex Cd(II), Pb(II), Cu(II) and Hg(II) cations in aqueous solutions with concentrations between 10^{-9} and 10^{-4} M has been proved. It was shown that **L**-CMEs can be successfully used to develop electrochemical sensors for the determination of Pb (II) and Cd(II) ions. The response was linear on the concentration range from 10^{-9} to 10^{-8} M and from 10^{-7} to 10^{-6} M for the analysis of Pb(II) and Cd(II) ions, respectively. The slope of 1.112 VA/M obtained for Pb(II) ion indicates a bigger sensitivity for this ion, which led to the most intense analytical signal. The detection limit for Pb(II) was estimated at 10^{-9} M, but this value can be optimized. This limit is much better from an analytical point of view than those obtained using other azulene ligands. The comparative results show the importance of the ligand structure in the design of molecular sensors, and the comparison between the **L**-CME study and the complexation study in solution showed the strong influence of the immobilization of the ligands through electropolymerization. Systematic studies on the optimization of preparation step for the obtained sensors based on **L**-CMEs are in progress in view of decreasing the detection limit under 10^{-9} M for Pb.

Supplementary Materials: The following are available online at https://www.mdpi.com/article/10.3390/sym13091642/s1, Figure S1: CV curves (0.1 V s^{-1}) recorded after the transfer of the modified poly-**L** electrodes in ferrocene solution (5 mM) in 0.1 M TBAP/CH_3CN compared to those recorded on bare electrode (dashed line); the modified electrodes were prepared by CPE (1 mC) at +0.8 V (red line) and +1.08 V (black line); Table S1: CV parameters for the curves in Figure S1; Figure S2: DPV curves for **L**-CMEs in 0.1 M TBAP, CH_3CN prepared in 1 mM solution of **L** in 0.1 M TBAP, CH_3CN by CPE at: +1.3 V, 1 mC (A) and at +0.8 V, 0.725 mC (B); Figure S3. CV curves for **L**-CMEs in 0.1 M TBAP, CH_3CN at different scan rates (V/s): 0.01—blue; 0.05—red; 0.1—green; 0.2—magenta; 0.3—cyan; 0.4—black; **L**-CMEs were prepared in 1 mM solution of **L** in 0.1 M TBAP, CH_3CN by CPE at: +1.3 V, 1 mC (A) and at +0.8 V, 0.725 mC (B) and Figure S4. Dependence of peak currents on the scan rate from CV curves for **L**-CMEs in 0.1 M TBAP, CH_3CN at different scan rates (V/s). **L**-CMEs were prepared in 1 mM solution of **L** in 0.1 M TBAP, CH_3CN by CPE at +1.3 V, 1 mC (A) and at +0.8 V, 0.725 mC (B).

Author Contributions: Conceptualization, E.-M.U.; validation, E.-M.U. and M.E.; formal analysis, L.-B.E., C.L., O.-T.M. and V.A.; investigation, L.-B.E., O.-T.M., A.G.B. and V.A.; complexation data analysis, C.-A.A. and J.B.; data curation, C.L.; writing—original draft preparation, C.-A.A., L.-B.E.

and V.A.; writing—review and editing, M.E., A.G.B., E.-M.U., C.L. and J.B.; supervision, E.-M.U.; resources E.-M.U. and M.E.; project administration, M.E. All authors have read and agreed to the published version of the manuscript.

Funding: This research was funded by UEFISCDI Romanian projects: 39PCCDI/2018 INTELMAT, PN-III-P1-1.1-TE-2016-0860, contract number 114/2018; 8BM/2019 PN-III-P3-3.1-PM-RO-FR-2019-0309; ECSEL-H2020, OCEAN12 (Ctr. number 9/1.1.3H/20.01.2020, POC-SMIS code 129948) and MADEin4 (Ctr. number 8/1.1.3H/06.01.2020, POC-SMIS code 128826).

Institutional Review Board Statement: Not applicable.

Informed Consent Statement: Not applicable.

Data Availability Statement: Available data are presented in the supplementary materials.

Acknowledgments: The authors address sincere thanks to the synthesis team from the Centre for Organic Chemistry, C. D. Nenitescu of the Romanian Academy coordinated by Alexandru C. Razus and by the regretted researcher Liviu Birzan (d. 2020).

Conflicts of Interest: The authors declare no conflict of interest.

References

1. Turdean, G.L. Design and Development of Biosensors for the Detection of Heavy Metal Toxicity. *Int. J. Electrochem.* **2011**, *2011*, 1–15. [CrossRef]
2. Jaishankar, M.; Tseten, T.; Anbalagan, N.; Mathew, B.B.; Beeregowda, K.N. Toxicity, mechanism and health effects of some heavy metals. *Interdiscip. Toxicol.* **2014**, *7*, 60–72. [CrossRef]
3. Afkhami, A.; Soltani-Felehgari, F.; Madrakian, T.; Ghaedi, H.; Rezaeivala, M. Fabrication and application of a new modified electrochemical sensor using nano-silica and a newly synthesized Schiff base for simultaneous determination of Cd2+, Cu2+ and Hg2+ ions in water and some foodstuff samples. *Anal. Chim. Acta* **2013**, *771*, 21–30. [CrossRef]
4. Tag, K.; Riedel, K.; Bauer, H.-J.; Hanke, G.; Baronian, K.H.; Kunze, G. Amperometric detection of Cu2+ by yeast biosensors using flow injection analysis (FIA). *Sens. Actuators B Chem.* **2007**, *122*, 403–409. [CrossRef]
5. Buica, G.-O.; Ungureanu, E.-M.; Birzan, L.; Razus, A.C.; Bujduveanu, M.-R. Films of poly(4-azulen-1-yl-2,6-bis(2-thienyl)pyridine) for heavy metal ions complexation. *Electrochim. Acta* **2011**, *56*, 5028–5036. [CrossRef]
6. Philips, M.F.; Gopalan, A.I.; Lee, K.-P. Development of a novel cyano group containing electrochemically deposited polymer film for ultrasensitive simultaneous detection of trace level cadmium and lead. *J. Hazard. Mater.* **2012**, *237–238*, 46–54. [CrossRef] [PubMed]
7. Kuddannaya, S.; Bao, J.; Zhang, Y. Enhanced In Vitro Biocompatibility of Chemically Modified Poly(dimethylsiloxane) Surfaces for Stable Adhesion and Long-term Investigation of Brain Cerebral Cortex Cells. *ACS Appl. Mater. Interfaces* **2015**, *7*, 25529–25538. [CrossRef]
8. Arrigan, D. Tutorial review. Voltammetric determination of trace metals and organics after accumulation at modified elec-trodes. *Analyst* **1994**, *119*, 1953. [CrossRef]
9. Bansod, B.K.; Kumar, T.; Thakur, R.; Rana, S.; Singh, I. A review on various electrochemical techniques for heavy metal ions detection with different sensing platforms. *Biosens. Bioelectron.* **2017**, *94*, 443–455. [CrossRef]
10. Hanrahan, G.; Patil, D.G.; Wang, J. Electrochemical sensors for environmental monitoring: Design, development and applications. *J. Environ. Monit.* **2004**, *6*, 657–664. [CrossRef]
11. Wang, F.; Lai, Y.-H.; Han, M.-Y. Stimuli-Responsive Conjugated Copolymers Having Electro-Active Azulene and Bithiophene Units in the Polymer Skeleton: Effect of Protonation and p-Doping on Conducting Properties. *Macromolecules* **2004**, *37*, 3222–3230. [CrossRef]
12. Wakabayashi, S.; Uchida, M.; Tanaka, R.; Habata, Y.; Shimizu, M. Synthesis of Azulene Derivatives That Have an Azathiacrown Ether Moiety and Their Selective Color Reaction Towards Silver Ions. *Asian J. Org. Chem.* **2013**, *2*, 786–791. [CrossRef]
13. Enache, L.-B.; Anăstăsoaie, V.; Birzan, L.; Ungureanu, E.-M.; Diao, P.; Enachescu, M. Polyazulene-Based Materials for Heavy Metal Ion Detection. 2. (E)-5-(azulen-1-yldiazenyl)-1H-Tetrazole-Modified Electrodes for Heavy Metal Sensing. *Coatings* **2020**, *10*, 869. [CrossRef]
14. Oprisanu, A.; Ungureanu, E.M.; Isopescu, R.; Birzan, L.; Mihai, M.; Vasiliu, I.C. Polyazulene based materials for heavy metal ions detection. *IOP Conf. Ser. Mater. Sci. Eng.* **2017**, *213*, 012050. [CrossRef]
15. Păun, A.-M.; Matica, O.-T.; Anăstăsoaie, V.; Enache, L.-B.; Diacu, E.; Ungureanu, E.-M. Recognition of Heavy Metal Ions by Using E-5-((5-Isopropyl-3,8-Dimethylazulen-1-yl) Dyazenyl)-1H-Tetrazole Modified Electrodes. *Symmetry* **2021**, *13*, 644. [CrossRef]
16. Pop, M.D.; Brincoveanu, O.; Cristea, M.; Buica, G.O.; Enachescu, M.; Ungureanu, E.M. AFM and SEM Characterization of Chemically Modified Electrodes Based on 5-[(azulen-1-yl) methylene]-2-thioxothiazolidin-4-one. *Rev. Chim.* **2018**, *68*, 2799–2803. [CrossRef]

17. Liu, D.; Huang, G.; Huang, C.; Huang, X.; Chen, J.; You, X. Cadmium Coordination Polymers Constructed from in Situ Generated Amino-Tetrazole Ligand: Effect of the Conditions on the Structures and Topologies. *Cryst. Growth Des.* **2009**, *9*, 5117–5127. [CrossRef]
18. Yao, Y.-L.; Xue, L.; Che, Y.-X.; Zheng, J.-M. Syntheses, Structures, and Characterizations of Two Pairs of Cd(II)-5-Aminotetrazolate Coordination Polymers. *Cryst. Growth Des.* **2009**, *9*, 606–610. [CrossRef]
19. Tseng, T.-W.; Luo, T.-T.; Chen, S.-Y.; Su, C.-C.; Chi, K.-M.; Lu, K.-L. Porous Metal–Organic Frameworks with Multiple Cages Based on Tetrazolate Ligands: Synthesis, Structures, Photoluminescence, and Gas Adsorption Properties. *Cryst. Growth Des.* **2012**, *13*, 510–517. [CrossRef]
20. Kang, X.-M.; Tang, M.-H.; Yang, G.-L.; Zhao, B. Cluster/cage-based coordination polymers with tetrazole derivatives. *Chem. Rev.* **2020**, *422*, 213424. [CrossRef]
21. Shimoni-Livny, L.; Glusker, J.P.; Bock, C.W. Lone Pair Functionality in Divalent Lead Compounds. *Inorg. Chem.* **1998**, *37*, 1853–1867. [CrossRef]
22. Birzan, L.; Cristea, M.; Tecuceanu, V.; Hanganu, A.; Ungureanu, E.-M.; Razus, A.C. 5-(Azulen-1-yldiazenyl)tetrazoles; Syntheses and Properties. *Rev. Chim.* **2020**, *71*, 251–264. [CrossRef]
23. March, G.; Nguyen, T.D.; Piro, B. Modified Electrodes Used for Electrochemical Detection of Metal Ions in Environmental Analysis. *Biosensors* **2015**, *5*, 241–275. [CrossRef] [PubMed]
24. Ungureanu, E.-M.; Razus, A.C.; Birzan, L.; Cretu, M.-S.; Buica, G.-O. Electrochemical study of azo–azulene compounds. *Electrochim. Acta* **2008**, *53*, 7089–7099. [CrossRef]
25. Gans, P.; Sabatini, A.; Vacca, A. Investigation of equilibria in solution. Determination of equilibrium constants with the HYPERQUAD suite of programs. *Talanta* **1996**, *43*, 1739–1753. [CrossRef]
26. Alderighi, L.; Gans, P.; Ienco, A.; Peters, D.; Sabatini, A.; Vacca, A. Hyperquad simulation and speciation (HySS): A utility program for the investigation of equilibria involving soluble and partially soluble species. *Coord. Chem. Rev.* **1999**, *184*, 311–318. [CrossRef]